COMPARISON OF TWO MODELING APPROACHES FOR SEMI-TRANSPARENT PHOTOVOLTAIC CLADDING IN GREENHOUSES AND EXPERIMENTAL CALIBRATION

Bambara J. and Athienitis A.K.
Centre for Zero Energy Building Studies
Concordia University, 1515 St. Catherine W., Montreal, H3G 2W1, Canada

ABSTRACT

Semi-transparent photovoltaics (STPV) can be employed as a greenhouse cladding material as a means to transmit sunlight while providing some shading and solar electricity generation. As such, this paper seeks to compare and experimentally calibrate two modeling approaches for STPV cladding using crystalline-silicon PV cells. The "separate" STPV model considers the PV cells as an exterior wall, while the "effective" STVP model employs an effective layer to represent the optical properties of the combined PV cell and clear-glazed sections. The predicted greenhouse air temperatures are found to be nearly identical for both STPV models, and both are in good agreement (±1°C) with the experimental measurements. However, the "effective" STPV model underestimated the PV cell temperature by approximately 10°C, resulting in a 5.1% overestimation of electric power output. Therefore, it is recommended that electric power be calculated based on a reference PV cell temperature. The "effective" STPV model is to be preferred over the "separate" model, as it is more advantageous for simulating blinds, thermal screens, and bi-facial PV cells.

INTRODUCTION

Building façades and roofs receive significant amounts of solar radiation, which can be used to generate useful energy on-site. This recent niche application involves PV greenhouses, which combine crop production and solar-based electricity generation. By covering the lower perimeter wall of the structure, PV cladding systems can be integrated onto greenhouses without affecting the sunlight received by the crop. Opaque and semi-transparent PV claddings can also be installed on the walls and roof, representing other promising applications. The reduction in the amount of sunlight transmitted will typically result in lower yield for most fruiting crops. However, leafy green vegetables often receive more sunlight than they require (particularly during the summer months and for low-latitude locations), and therefore shading devices are commonly used to prevent damage by excessive heat and sunlight. Semi-transparent photovoltaics (STPV) can be employed as a greenhouse cladding material as a means to transmit a fraction of sunlight while providing both shading and solar electricity production. The solar electricity that is generated constitutes their main advantage over movable shading devices; however, the fixed nature of STPVs can also reflect a disadvantage, as the amount of sunlight transmitted cannot be adjusted. In Europe, opaque PV and STPV cladding have been employed to cover the south-facing roofs of greenhouses following an east–west orientation (Fig. 1).

Fig. 1: STPV modules covering south-facing roof of a greenhouse in Montélimar, France (Tritec, 2015).

Commercially available STPV modules are comprised of crystalline-silicon PV cells that are encapsulated between an exterior glazing and an interior glazing, or transparent plastic film. Promising STPV modules for advanced greenhouses include the frameless glass-glass modules commercialized by Canadian Solar (2015). Ideally, long and narrow crystalline-silicon PV cells should be used to minimize shading patches over the crop. Recently, thin-film and organic STPV technologies have been considered for low-cost greenhouse applications due to their transparent, flexible, and lightweight properties (Emmott *et al.*, 2015). Solar electricity can also be generated from the solar radiation that is transmitted and reflected onto the interior surfaces using bi-facial PV cells.

A major design parameter for STPV cladding is the portion of the glazed area that is covered by crystalline-

silicon PV cells (PV area ratio). For thin-film and organic STPV modules, transparency is used (instead of PV area ratio) to describe the amount of sunlight that is transmitted by the glazing. A major drawback of STPV compared to blinds is that they cannot be withdrawn during cloudy days or in winter, when light is limited; this means that the PV area ratio needs to be optimized for the crop being produced. When artificial lighting is used, the annual increase of lighting energy should be weighed against the PV electric energy generation. Depending on the geographic location, the electric energy production can exceed the greenhouse energy demand. This surplus electricity can either be used by adjacent/neighbouring buildings, exported to the grid, or stored for later use on-site. Ganguly and Ghosh (2011) investigated the use of a PEM electrolyser to convert excess electricity from a PV greenhouse into hydrogen, which is then stored and used in a fuel cell to generate needed electricity at a later time.

Researchers are increasingly investigating the effects of various PV area ratios (or transparency) on the energy performance and crop yield of greenhouses. A greenhouse equipped with STPV cladding was modeled by Carlini *et al.* (2012) using TRNSYS simulation software, and annual simulations were used to compare the energy consumption of a greenhouse with and without STPV. It was found that heating and cooling could be reduced by 11% and 30%, respectively. There was no yield reduction observed with tomato crops inside a greenhouse with a 9.8% PV area ratio, despite negative effects observed on the fruit size and colour (Ureña-Sánchez, 2012). A crop yield loss of 25% was observed for Welsh onions when a PV area ratio of 13% was used (Kadowaki, 2012). The biomass production and yield of basil and zucchini crops were not affected significantly by a PV area ratio of approximately 20% (Minuto, 2009).

Detailed energy models of greenhouses employing STPV cladding are required in order to obtain optimal designs that take into account both energy performance and crop yield. Several approaches have been proposed for modeling STPV cladding using custom models (Robinson, 2009), TRNSYS (Carlini *et al.*, 2012), EnergyPlus (Peng *et al.*, 2015), and computational fluid dynamics (Fatnassi *et al.*, 2015). For the modeling STPV cladding employing crystalline-silicon PV cells, a common approach is to use an effective layer to represent the optical properties of the combined PV cell and clear-glazed sections. However, this approach underestimates PV cell temperature (PV cells are no longer considered opaque), resulting in an overestimation of PV electric energy power output.

The objective of this paper is to compare two modeling approaches for STPV modules, employing crystalline-silicon PV cells with measurements obtained from an experimental greenhouse mock-up. The advantages and drawbacks of using each modeling approach for predicting the thermal and electric energy performance are identified and presented, including the potential ways to address limitations. In addition, the most suitable modeling approach is defined for the cases where blinds, thermal screens, and bi-facial PV cells are considered as design options.

EXPERIMENT

The Concordia University Paul Fazio Solar Simulator - Environmental Chamber (SSEC) laboratory is an indoor research facility designed to emulate outdoor weather conditions (solar radiation, exterior air temperature, wind, etc.). It therefore provides a fully controlled and monitored environment for research, development, and testing of solar energy applications and advanced building envelopes. A 4.65 m^2 experimental greenhouse concept integrated with STPV cladding (2.37 m x 1.96 m x 2.03 m) was built (Fig. 2). Six 58 Watt STPV modules (45.5% PV cells, 49.2% clear glazing and 5.3% framing) are used to cover one of the walls.

Fig. 2: Photo of the experimental greenhouse.

During testing, the greenhouse is placed inside the environmental chamber, which is maintained at an air temperature of between 6-9°C (Fig. 3). Then, the solar simulator lampfield is used to transmit shortwave radiation through the environmental chamber (EC) windows and onto the STPV wall of the experimental

greenhouse. The lampfield uses a set of six metal halide global (MHG) lamps, with a total peak power output of 27.6 kW. The MHG lampfield produces a dense multiline spectrum of rare earth metals similar to the air mass 1.5 spectrum defined by EN 60904-3. This provides a spectral distribution very close to natural sunlight, and fulfils the specifications of relevant standards EN 12975:2006 and ISO 9806-1:1994 (PSE, 2009). The lamps can also be individually moved on 2 axes and dimmed, offering the possibility to illuminate test surfaces of different sizes with variable degrees of irradiance intensity. In this experiment, an average irradiance of 1038 W/m^2 was provided on the STPV wall with a distribution uniformity of 86%. Irradiance is measured by a pyranometer by PSE, mounted on an X-Y collector scanner with an accuracy of ± 5% of the reading. Two fans are used to mix the air within the greenhouse.

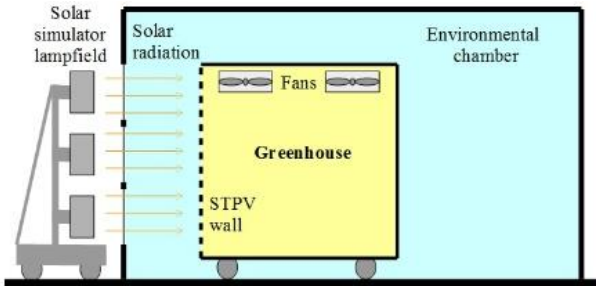

Fig. 3: Experimental setup inside the SSEC laboratory.

The STPV cladding is made of 156 mm square polycrystalline-silicon PV cells, encapsulated between 3.2 mm low-iron patterned (diffusing) clear glass on the exterior and a polyvinyl fluoride film on the interior. The framing consists of aluminum approximately 4 mm thick. The walls and roof are made of 4 mm extruded polypropylene sheets that are fastened to a 38 mm x 89 mm softwood framing located on the exterior, so that its effects on heat transfer are minimized. The floor is constructed of 38 mm x 140 mm softwood joists that are covered by 19 mm plywood, with 4 mm extruded polypropylene sheets used as the interior finish. The experiment is mounted on wheels which elevate it by approximately 150 mm above the floor level. The walls, floor, and roof are painted black with a matte finish.

The greenhouse air temperature and PV cell surface temperatures were measured using T-Type thermocouples with an accuracy of ± 0.3°C. Air temperatures were taken as the average of 15 thermocouples (five along the height at three locations), and the PV cell temperature was measured on the interior for six cells (three along the height at two locations). The average EC air temperature and interior surface temperatures were also measured for the lampfield windows, front, back, side walls, roof, and floor. The rate of direct current (DC) electric energy generated by the six STPV modules (wired in series) was determined by measuring the produced current and voltage using an IV curve tracer (DS-100C by Daystar inc.). The error in measured voltage is the larger of ± 0.5% of reading or ± 0.028 Volts. The error in measured current is the larger of ± 0.5% of reading or ± 0.045 Amps. An electronic load (eload) device (N3300A by Agilent) was used as an electric load. The eload was configured to allow the STPV panels to operate at the maximum power point measured by the IV tracer.

The data acquisition system is made up of one CompactRIO device fabricated by National Instruments. The CompactRIO chassis uses NI 9211 thermocouple input modules to convert the analogue voltage signal from the sensor into a storable digital signal. The CompactRIO device was connected to a desktop computer running National Instruments' LabVIEW software. A program running inside LabVIEW was designed to provide a real-time graphical display and to record data on the computer's hard drive. The data was sampled every 10 seconds and recorded as one-minute averages.

The experimental testing began when the greenhouse air temperature was in equilibrium with the EC air. The mixing fans and the solar simulator lampfield were simultaneously turned on. Approximately two hours into the experiment, the PV modules were disconnected from the load for a period of 30 minutes so that the effect of the PV electric power output on the thermal performance could be assessed. About 3 hours into the experiment, the solar simulator lampfield was turned off.

MODELING AND SIMULATION

TRNSYS 17.2, which has a modular structure, is selected as the simulation software for the transient simulation of systems (TRNSYS, 2012). A TRNSYS project is typically set up by connecting components graphically in the Simulation Studio. TRNSYS components are often referred to as "Types," which are described by a mathematical model in the TRNSYS simulation engine (TRNSYS, 2012; TESS, 2014). Type 56 was originally developed to model multizone buildings and is used here with certain assumptions to create the greenhouse energy model (TRNSYS, 2005). The visual interface for Type 56 is called TRNBuild. The greenhouse geometry was defined in Sketchup (Sketchup, 2015) and imported into TRNBuild in order to provide detailed radiation calculations using view

factor matrices. The set of equations for heat transfer from and within the zone are formulated in a matrix in Type 56 and solved at each simulation time-step. Based on the need to calibrate an energy model using measurements from the experiment, a short time-step of one minute is selected for the simulations. Fig. 4 illustrates the major energy fluxes considered in the greenhouse model.

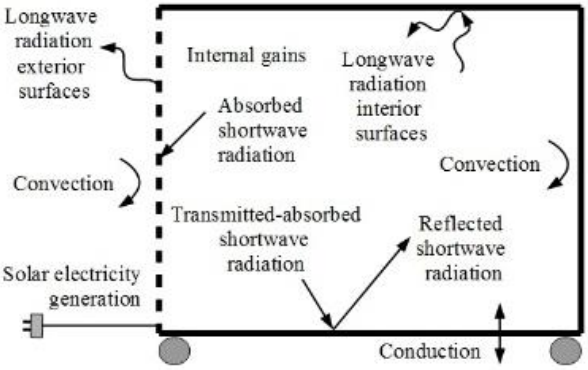

Fig. 4: Schematic showing energy fluxes considered in the greenhouse model.

The mass balance for the greenhouse airnode is not considered, because there is no ventilation and infiltration is neglected (all joints were sealed with silicone, and a door with continuous weather stripping was used).

The energy balance for the greenhouse airnode can be written as:

$$MF \cdot \rho_{air} \cdot c_{p\_air} \cdot V_{gh} \cdot \frac{\partial T_{gh}}{\partial t} = \dot{Q}_{conv\_i} + \dot{Q}_{gains} \qquad (1)$$

Where
MF is the capacitance multiplication factor;
ρ_{air} is the density of air;
c_{p_air} is the specific heat of air at constant pressure;
V_{gh} is the greenhouse volume;
$\frac{\partial T_{gh}}{\partial t}$ is the rate of change of the airnode temperature with respect to time;
$\dot{Q}_{conv\_i}$ is the convection heat flux between the airnode and the interior surfaces and;
$\dot{Q}_{gains}$ are the internal gains.

The energy balance for a given interior surface (walls, roof and floor) can be written as:

$$0 = \dot{Q}_{abs\_i} + \dot{Q}_{conv\_i} + \dot{Q}_{rad\_i} + \dot{Q}_{cond} \qquad (2)$$

Where
$\dot{Q}_{abs\_i}$ is the shortwave radiation that is transmitted and absorbed on the interior surface;
$\dot{Q}_{rad\_i}$ is the longwave radiation heat flux between the surface and other interior surfaces and;
$\dot{Q}_{cond}$ is the conduction heat transfer between the exterior and interior surfaces.

The energy balance for a given exterior surface (walls, roof and floor) can be written as:

$$0 = \dot{Q}_{conv\_o} + \dot{Q}_{rad\_o} + \dot{Q}_{cond} \qquad (3)$$

Where
$\dot{Q}_{conv\_o}$ is the convection heat flux between the ambient air and the exterior surface and;
$\dot{Q}_{rad\_o}$ is the longwave radiation heat flux between the exterior surface and the viewing surface (interior surfaces of the EC).

The STPV wall is modeled using two different approaches, termed the "separate" and "effective" STPV models, for comparison. A description of each model follows.

The "separate" STPV model considers distinct treatment of the PV cell area, clear-glazed area, and frame. The PV cell area is modeled as an exterior wall that surrounds a window comprised of a clear glazing and frame (Fig. 5).

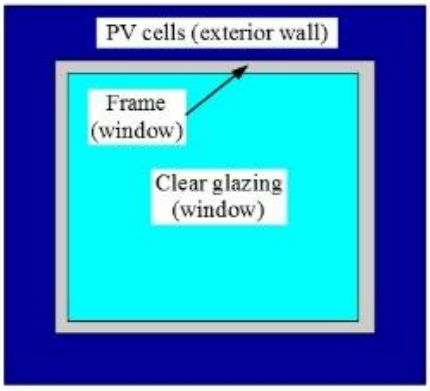

Fig. 5: Schematic showing the defined surfaces for the "separate" STPV model.

The thermal resistance and capacitance is ignored for the PV cell wall, and the energy balance on its surface can be written as:

$$0 = \dot{Q}_{abs\_o} + \dot{Q}_{conv\_o} + \dot{Q}_{rad\_o} + \dot{Q}_{cond} - \dot{E}_{pv} \quad (4)$$

Where
$\dot{Q}_{abs\_o}$ is the incident shortwave radiation absorbed on the exterior surface of the glazing and;
$\dot{E}_{pv}$ is the PV electric power output.

The thermal resistance and capacitance is ignored for the clear-glazed window, and the energy balance on its surface can be written as:

$$0 = \dot{Q}_{abs\_o} + \dot{Q}_{abs\_i} + \dot{Q}_{conv\_i} + \dot{Q}_{rad\_i} + \dot{Q}_{conv\_o} + \dot{Q}_{rad\_o} \quad (5)$$

The energy balance of the exterior surface of the frame, ignoring its capacitance, can be written as:

$$0 = \dot{Q}_{abs\_o} + \dot{Q}_{conv\_o} + \dot{Q}_{rad\_o} + \dot{Q}_{cond} \quad (6)$$

The energy balance of the interior surface of the frame, ignoring its thermal capacitance, can be written as:

$$0 = \dot{Q}_{abs\_i} + \dot{Q}_{conv\_i} + \dot{Q}_{rad\_i} + \dot{Q}_{cond} \quad (7)$$

The "effective" STPV model considers the combination of PV cell and clear-glazed portions into an effective layer. The optical properties of the effective STPV layer are calculated using an area-weighted approach based on the clear-glazed portion and opaque portion covered by PV cells (see "modeling key assumptions" section later). The energy balance for the effective STPV surface, neglecting its thermal resistance and capacitance, can be written as:

$$0 = \dot{Q}_{abs\_o} + \dot{Q}_{abs\_i} + \dot{Q}_{conv\_o} + \dot{Q}_{conv\_i} + \dot{Q}_{rad\_o} + \dot{Q}_{rad\_i} - \dot{E}_{pv} \quad (8)$$

Type 56 requires that at least 1% of a surface be defined as a wall (i.e. maximum 99% window). Therefore, this wall surface is modeled as a PV cell (same as for the "separate" model) and can be used as a reference for calculating the temperature-dependent electric power output.

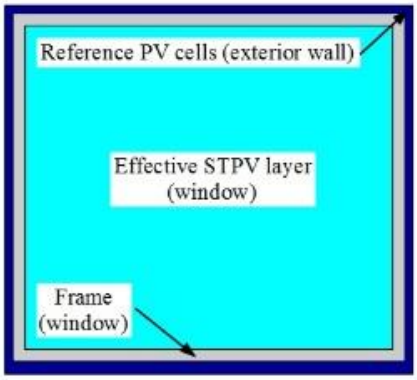

Fig. 6: Schematic showing the defined surfaces for the "effective" STPV model.

Modeling key assumptions

Conduction: Conduction heat transfer occurs through the building envelope (walls, floor, roof, and windows). Conduction is calculated based on the one-dimensional transient heat conduction equation for a thin element (∂x) and for constant conductivity given by:

$$\frac{\partial^2 T}{\partial x^2} = \frac{1}{\alpha} \cdot \frac{\partial T}{\partial t} \quad (9)$$

Where
∂T is the change in temperature;
∂t is the time interval and;
α is the thermal diffusivity of the material given by:

$$\alpha = \frac{k}{\rho \cdot C_p} \quad (10)$$

Where k, ρ and C_p are the thermal conductivity, density, and specific heat of the material, respectively.

Type 56 uses the transfer function method to solve the transient conduction heat transfer ($\dot{Q}_{cond}$) through the opaque envelope components (Stephenson and Mitalas, 1971; Mitalas and Arseneault, 1972). Thermal capacitance is neglected for heat conduction through the window glazing and frame, and one-dimensional steady state heat conduction is given by:

$$\dot{Q}_{cond} = U \cdot A \cdot \Delta T \quad (11)$$

Where
U is the layer thermal conductance
A is the surface area and;
ΔT is the temperature difference across the layer.

The thermal capacitance of the window (glazing and frame), PV cells, and extruded polypropylene is ignored. The thermal conductance of the glazing (clear glazing,

PV cell wall, and effective STPV layer) and frame is estimated to be 232 W/(m^2·K). The thermal conductance of the extruded polypropylene was measured to be 11.3 W/(m^2·K). The thermal mass of the plywood that was installed on the floor is considered with thermal conductance, specific heat, and density estimated to be 7.9 W/(m^2·K), 1200 J/(kg·K), and 800 kg/m^3, respectively. The edge effects and framing are ignored in the model.

Convection: The greenhouse envelope generally has low thermal resistance, and thus convection heat transfer has a significant impact on heat transfer. The convection heat flux is given by:

$$\dot{Q}_{conv} = h_i \cdot A_i \cdot (T_i - T_{air}) \quad (12)$$

Where
h_i is the average interior convective heat transfer coefficient (CHTC);
A_i is the surface area;
T_i is the surface temperature and;
T_{air} is the air temperature, taken as the greenhouse air temperature for interior CHTC and the EC air temperature (ambient air) for the exterior CHTC.

The interior CHTC is estimated to be 10 W/(m^2·°C) for the walls (opaque and STPV), roof, and floor. The exterior CHTC are estimated to be 8 W/(m^2·°C) for the walls and roof, and 5 W/(m^2·°C) beneath the floor.

Longwave radiation: Longwave radiation heat transfer plays an important role in highly glazed buildings such as greenhouses, where large differences in interior surface temperature occur. Detailed radiation heat transfer calculations are performed by considering the radiation exchange of a given surface with all other viewing surfaces (as opposed to the starnet method, which uses a combined radiative and convective heat transfer coefficient). Longwave radiation heat flux between two surfaces is given by:

$$\dot{Q}_{rad} = F_{i,j} \cdot \varepsilon_i \cdot \sigma \cdot A_i \cdot \left(T_j^4 - T_i^4\right) \quad (13)$$

Where
$F_{i,j}$ is the view factor between a given surface (i) at temperature T_i, and other viewing surfaces (j) at temperature T_j;
ε_i is the surface emissivity;
σ is the Stefan-Boltzmann constant and;
A_i is the surface area.

For longwave radiation exchange on exterior surfaces, the viewing surfaces include the average EC interior surface temperatures (for all surfaces except the STPV wall) and the area-weighted average EC interior lampfield wall and window temperature (for the STPV wall). Type 56 enables detailed radiation calculations for building geometries that are convex. Sketchup is used to create three-dimensional data of the building, then the view factor matrices (for interior surfaces) are generated in TRNBuild, and the longwave radiation heat transfer is calculated using the so-called Gebhart-factor (Gebhart, 1961; 1971).

The emissivity for the interior and exterior surfaces of the extruded polypropylene and PV cells, and the exterior surface of the floor, are assumed to be 0.9. The emissivity of the clear glazing and aluminum frame are assumed to be 0.84 and 0.77, respectively.

Shortwave radiation: Greenhouse glazing transmits large amounts of solar radiation, which is absorbed and reflected by the interior surfaces. The energy balance is also affected by solar radiation that is absorbed by the exterior window frames and perimeter walls. The shortwave radiation produced by the solar simulator lampfield is modeled as a diffuse radiation that is incident on the STPV wall because of the patterned glass. The measured average irradiance of 1038 W/m^2 is used in the model. For a detailed treatment of shortwave diffuse radiation including multi-reflection, the view factor matrices and so-called Gebhart-factor are used.

The absorptance of shortwave radiation on the interior surface of the extruded polypropylene (black paint), clear glazing, frame, and interior surface of the PV cells is assumed to be 0.9, 0.05, 0.15, and 0.3, respectively. The absorptance-transmittance of the exterior surface of the PV cells is assumed to be 0.85. The average transmittance of the clear-glazed portion was measured to be 0.77.

Internal gains: The sensible heat gains considered in the model are equal to the heat produced by two air mixing fans, given by:

$$\dot{Q}_{gains} = \dot{E}_{fan} \quad (14)$$

Where $\dot{E}_{fan}$ is the power of the two mixing fans, measured to be 66.7 Watts each using a handheld Watt-meter.

PV electric power: The electric power produced by the PV affects the surface energy balance, and therefore it is modeled as a heat loss equal to the measured rate of DC electric power output, given by:

$$\dot{E}_{meas} = V_{meas} \cdot I_{meas} \quad (15)$$

Where
V_{meas} is the measured DC voltage across the STPV string and;
I_{meas} is the measured DC current through the STPV string.

The error in the reported electric power is given by:

$$\Delta\dot{E}_{meas} = \sqrt{(\Delta V_{meas})^2 \cdot (\Delta I_{meas})^2} \quad (16)$$

Where
ΔV_{meas} is the error in measured voltage from the IV curve tracer and;
ΔI_{meas} is the error in measured current from the IV curve tracer.

The measured electrical efficiency of the STPV string is given by:

$$\eta_{meas} = \frac{\dot{E}_{meas}}{\dot{G}_{meas} \cdot A_{PV}} \quad (17)$$

Where
$\dot{G}_{meas}$ is the measured incident shortwave radiation and;
A_{PV} is the total PV cell area (2.19 m^2).

The error in the reported electrical efficiency is given by:

$$\Delta\eta_{meas} = \sqrt{\left(\Delta\dot{E}_{meas}\right)^2 + \left(\Delta\dot{G}_{meas}\right)^2} \quad (18)$$

Where
ΔG_{meas} is the error in measured incident shortwave radiation from the pyranometer.

The minimum measured value of irradiance over the STPV wall (926.5 W/m^2) is used for PV electric energy calculations because it dictates the current produced by the STPV modules that were wired in series.

The theoretical temperature-dependent rate of DC electric energy generated by the PV surface is given by (Skoplaki and Palyvos, 2009):

$$\dot{E}_{theo} = \dot{G} \cdot A_{PV} \cdot [\eta_{STC} \cdot (1 - \beta_{PV} \cdot \langle T_{PV} - T_{STC} \rangle)] \quad (19)$$

Where
$\dot{G}$ is the total incident shortwave radiation;
η_{STC} is the STPV module efficiency at standard testing conditions (STC);
β_{PV} is the STPV module temperature coefficient;
T_{PV} is the PV cell temperature and;
T_{STC} is the PV cell temperature at STC (25°C).

The effect of the wiring losses is not considered.

Custom windows: The program Window 7.3 is used to generate thermal and optical properties for custom window assemblies, comprised here of a single glazing and frame (DOE, 2015). The "separate" STPV model considers a clear glazing and frame, whereas the "effective" STPV model considers the effective STPV layer (PV cells and clear glazing) and frame. The output data of Window 7.3 is then used to define a new window in TRNBuild. Type 56 calculates the amount of shortwave radiation that is absorbed and transmitted by the glazing (here it includes the diffuse component and its reflections). It is assumed that the shortwave radiation transmitted through the STPV wall is diffuse. Energy storage in the glazing and frame are neglected.

"Effective" STPV layer: This STPV model is specified as a custom window in Type 56, where the glazed portion (comprised of a clear glazing and PV cell portion) is modeled as an effective layer whose optical properties depend on the PV area ratio. The transmittance (τ_e) and reflectance (ρ_e) of the effective STPV layer, for shortwave radiation directed from outside (o) to inside (i) and vice versa, can be calculated using the following equations:

$$\tau_{e\_o} = \tau_{g\_o} \cdot (1 - F_{PV}) \quad (20)$$

$$\tau_{e\_i} = \tau_{g\_i} \cdot (1 - F_{PV}) \quad (21)$$

$$\rho_{e\_o} = \rho_{PV\_o} \cdot F_{PV} + \rho_{g\_o} \cdot (1 - F_{PV}) \quad (22)$$

$$\rho_{e\_i} = \rho_{PV\_i} \cdot F_{PV} + \rho_{g\_i} \cdot (1 - F_{PV}) \quad (23)$$

Where
F_{PV} is the PV area ratio (0.48);
τ_{g_o} and τ_{g_i} are the transmittances of the clear glazing for the exterior and interior sides (0.77);
ρ_{PV_o} and ρ_{PV_i} are the PV reflectance for the exterior (0.15) and interior (0.7) sides and;
ρ_{g_o} and ρ_{g_i} are the clear glazing reflectance for the exterior and interior sides (0.18).

Based on equations 20-23, the transmittance of the effective STPV layer in both directions is 0.4, and the exterior and interior reflectance are 0.1 and 0.36, respectively. The effective absorptance for each side of the glazing is given by:

$$\alpha_e = 1 - \tau_e - \rho_e \quad (24)$$

Based on equation 24, the exterior and interior absorptance of the effective STPV layer are 0.5 and 0.24, respectively. The obtained effective transmittance and reflectance are then used to create a custom glazing in Window 7.3. The PV electric power output can be calculated in the same way as for the "separate" STPV model using a PV cell area equal to:

$$A_{PV} = F_{PV} \cdot \left(A_{STPV} - A_{frame}\right) \quad (25)$$

A similar modeling approach can be used to consider thin-film and organic STPV cladding, using transparency instead of the PV area ratio.

RESULTS AND DISCUSSION

The DC voltage across and the current through the STPV string (six STPV modules wired in series) was measured to be 36.8 ± 0.2 Volts and 6.08 ± 0.05 Amps, respectively (measured just before disconnecting them from the eload). The electric power output is 224.4 ± 0.01 Watts (equation 15-16), and the electrical efficiency of the STPV string is calculated to be 11.1 ± 0.006 % (equation 17-18).

Fig. 7 shows that the solar simulator radiation causes the average PV cell temperature to rise by 44°C and reach a steady state temperature of 50.4°C in approximately one hour. It also provides a comparison of the measured average PV cell temperature with those obtained using both STPV models. It is found that the "separate" STPV model is in good agreement (±1°C) with the measured results, whereas the "effective" STPV model underestimates the PV surface temperature by approximately 10°C. This result is expected because the effective STPV layer is semi-transparent and has a lower absorptance (0.5) than the PV cells modelled as an opaque wall (0.85). The main consideration is whether this has an impact on the greenhouse air temperature. This will be evaluated later.

Based on these measurements, the theoretical rate of electric energy generated by the STPV string is found to be 224.1 and 235.7 Watts, for the "standard" and "effective" STPV models, respectively (equation 19, with an input of 0.125 for the PV module electrical efficiency and of 0.0046 for the temperature coefficient (Athenitis *et al.*, 2011). Thus, the "standard" STPV model provides an accurate estimation of the electric power output (0.1% lower), whereas the "effective" STPV models overestimate it by 5.1%. A possible approach that can be used to avoid overestimating electric power output when using the "effective" STPV model is to define the wall around the STPV window (representing 1% of total surface area) as an exterior wall comprised of PV cells. This provides the same PV cell surface temperature as the "separate" STPV model (confirmed from the model results and therefore not presented here) and could be used as a reference for calculating a more realistic electric power. Since the greenhouse air temperature is nearly identical for both STPV models, it is assumed that the PV cell temperature would also be the same. It should be noted that this approach is only valid for STPV modules using crystalline-silicon PV cells. For thin-film and organic STPV modules, the "effective" STPV model provides a valid surface temperature for estimating electric power output (i.e. "separate" STPV model is not applicable).

Fig. 7 also shows that when the STPV string is disconnected from the load, the measured average PV cell temperature increases by 4.4°C (from 50.4 to 54.8°C). This demonstrates the importance of accounting for electric power production in the PV surface (PV wall and effective STPV layer) energy balance. Moreover, the effect of not considering the thermal capacitance of the STPV surface can be observed from the sharp rise/decay in the modeled surface temperature compared to the experimental measurements.

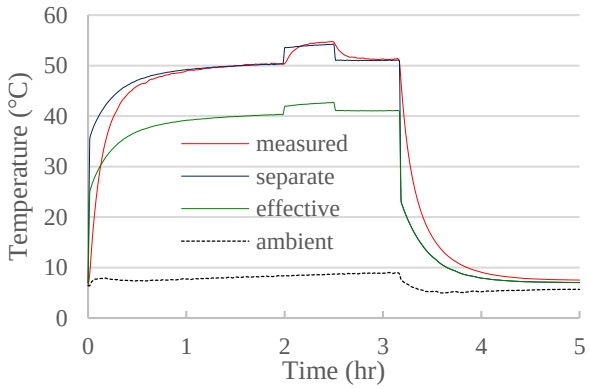

Fig. 7: Comparison of measured average PV cell temperature with those obtained using both STPV models.

Fig. 8 shows that the solar simulator radiation causes the greenhouse air temperature to rise by 26.2°C and reach a steady state temperature of 33.1°C in approximately one hour. It also provides a comparison of the measured average greenhouse air temperature with those obtained using both STPV models. The results indicate that good agreement (±1°C) exists between the measured and modeled results when an air capacitance multiplication factor of eight is used in the model. Most importantly, no noticeable difference can be observed between the

predictions obtained from the "separate" and "effective" STPV models. This suggests that, despite discrepancies in the PV surface temperature predictions, the "effective" STPV model accurately represents shortwave radiation transmitted by the STPV modules.

Moreover, the greenhouse air temperature increased by 1.4°C (from 33.1 to 34.5°C) when the STPV modules were disconnected from the load. This confirms that electric power production should be accounted for in the energy balance of the PV surface (PV wall and effective STPV layer) because it also affects the predicted greenhouse air temperature.

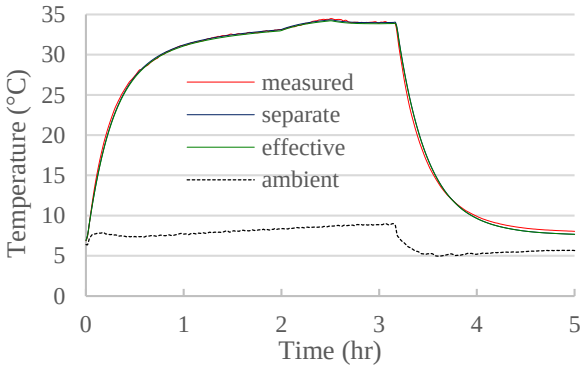

Fig. 8: Comparison of measured average greenhouse air temperature with predictions using both STPV models.

Based on these results, it is found that both STPV models can be used to accurately predict the air temperature inside a greenhouse equipped with crystalline-silicon STPV modules. However, the reference PV cell temperature should be used to accurately predict the temperature-dependent electric power output when the "effective" STPV model is selected. Moreover, it is recommended to use the "effective" STPV model for all types of STPV cladding (crystalline-silicon, thin-film, and organic) because it has the following advantages over its "separate" counterpart:

1) The PV area ratio (or transparency) can be easily modified using the "effective" STPV model. Custom windows representing STPV modules of various PV area ratios (and possibly multi-glazed STPV) can be created in Window 7.3 at the beginning of a project. It is then easy to change the STPV design for various surfaces in the building model (including the option of selecting a clear glazed window instead of STPV). For the "separate" STPV model, the geometry must be modified in SketchUp in order to increase or decrease the portion of the wall covered by PV cells, and then re-imported into TRNBuild, which is a tedious process.

2) Inter-reflections of shortwave radiation caused by the closing of a blind are accounted for by the "effective" STPV model. This is particularly important in greenhouse applications where interior blinds are commonly used. In addition, the "effective" STPV model allows a blind to be closed over the entire window area (comprised of PV cells, glazing and frame). For the "separate" STPV model, the blind can only be applied to the glazed surface (which excludes the PV cells), and reflection/absorption of shortwave radiation on the PV cells cannot be taken into account.

3) A detailed modeling of bi-facial PV cells that considers the inter-reflections of the blinds is possible using the "effective" STPV model. The closing of the blind causes much of the sunlight to be reflected on the interior side of the bi-facial solar cell, resulting in increased electric power output compared to when the blind is not in use. The "separate" STPV model can be employed to model single-glazed bi-facial PV cells that do not use a blind.

4) Detailed modeling of the convection and longwave radiation heat transfer is possible when a thermal screen is applied. The "effective" STPV model enables a thermal screen (modeled as a blind which closes at night) to be drawn across the entire window area (comprised of PV cells, glazing and frame). This allows for the consideration of the detailed modeling of convection, and most importantly, longwave radiation (Type 56 allows for us to specify the emissivity of the blind material). The "separate" STPV model cannot apply the thermal screen over the PV cell wall. A possible solution for considering the additional thermal resistance of the blind is to adjust the interior CHTC, but this does not account for the emissivity of the thermal screen.

CONCLUSIONS

This study compared and experimentally calibrated two modeling approaches for simulating STPV cladding, using TRNSYS Type 56. The predicted greenhouse air temperatures are found to be nearly identical for both STPV models, and they are in good agreement (±1°C) with the experimental measurements. However, the "effective" STPV model underestimated the PV cell temperature by approximately 10°C, resulting in a 5.1% overestimation of electric power output when compared to the "separate" STPV model. Therefore, both STPV

models can be used to predict the greenhouse air temperature, but adjustments are needed to accurately determine the temperature-dependent PV electric power output when the "effective" STPV model is selected. A proposed solution is to calculate PV electric power based on a reference PV cell temperature. Moreover, it is recommended to use the "effective" STPV approach for modeling all types of STPV claddings, since it enables us to compare various STPV designs: this approach can accurately model the use of blinds, thermal screens and bi-facial PV cells.

Detailed energy models for greenhouses that employ STPV cladding are needed in order to obtain optimal designs that take into account their effect on energy performance and crop yield. The integration of STPV cladding in greenhouses can improve the growing conditions for leafy green vegetables, while also representing a promising source of renewable energy.

ACKNOWLEDGEMENTS

The authors acknowledge the financial support of the Natural Sciences and Engineering Research Council of Canada through the Alexander Graham Bell Canada Graduate Scholarship, the NSERC Smart Net Zero Energy Buildings Strategic Research Network and the Concordia Institute for Water, Energy and Sustainable Systems. Thanks to Jiwu Rao, Jaime Yeargans, Joe Rhib and William Gagnon for their help with the experimental work and to Shawn Katz and Gerald Parnis for editing this paper.

NOMENCLATURE

A	surface area, m^2
C_p	specific heat at constant pressure, J/(kg·K)
$\dot{E}$	electric power consumed/produced, W
EC	environmental chamber
F	PV area ratio or view factor
$\dot{G}$	incident shortwave radiation, W/m^2
h	convective heat transfer coefficient, $W/(m^2 \cdot K)$
I	current, A
k	thermal conductivity, W/(m·K)
MF	capacitance multiplication factor
MHG	metal halide global
PV	photovoltaics
$\dot{Q}$	heat flux, W
SSEC	solar simulator - environmental chamber
STPV	semi-transparent photovoltaics
t	time, s
T	temperature, K
U	layer thermal conductance, $W/(m^2 \cdot K)$
V	volume, m^3 or voltage, V
α	thermal diffusivity, m^2/s or absorptance
β	PV module temperature coefficient, 1/K
Δ	error or difference
ε	surface emissivity
η	electrical efficiency, %
ρ	density, kg/m^3 or reflectance
σ	Stefan-Boltzmann constant, $W/(m^2 \cdot K^4)$
τ	transmittance

Subscripts

abs	absorbed or transmitted-absorbed
air	greenhouse air
cond	conduction
conv	convection
DC	direct current
e	effective
fan	mixing fan
frame	STPV frame
g	glazing
gains	internal gains
gh	greenhouse
i	inside surface
j	viewing surface
meas	measured
o	outside
PV	photovoltaic cells
rad	longwave radiation
STC	standard testing conditions
STPV	semi-transparent photovoltaics
theo	theoretical

REFERENCES

Athienitis A.K., Bambara J., O'Neill B., Faille J., (2011), A prototype photovoltaic/thermal system integrated with transpired collector. *Solar Energy*. 85(1) 139–153.

Canadian Solar, 2015. http://www.canadiansolar.com/solar-panels/cs6x-p-fg.html.

Carlini M., Honorati T. and Castellucci S. (2012), Photovoltaic Greenhouses: Comparison of Optical and Thermal Behaviour for Energy Savings. *Mathematical Problems in Engineering.* Article ID 743764.

DOE (2015), https://windows.lbl.gov/software/window/7/index_7_3_4.html

Emmott C.J.M., Röhr J.A., Campoy-Quiles M., Kirchartz T., Urbina A., Ekins-Daukesa N.J. and Nelson J. (2015), Organic photovoltaic greenhouses: a

unique application for semi-transparent PV? *Energy Environment Science*. 8 1317-1328.

Fatnassi H., Poncet C., Bazzano M.M., Brun R. and Bertin N. (2015), A numerical simulation of the photovoltaic greenhouse microclimate. *Solar Energy*, 120 575-584.

Ganguly A. and Ghosh S. (2011), Performance Analysis of a Floriculture Greenhouse Powered by Integrated Solar Photovoltaic Fuel Cell System. *Journal of Solar Energy Engineering.* 133 1-7.

Gebhart B. (1961), Surface Temperature Calculations in Radiant Surroundings of Arbitrary Complexity – for Gray, Diffuse Radiation. *International Journal of Heat and Mass Transfer*. 3(4) 341-346.

Gebhart B. (1971), *Heat Transfer*, 2nd ed. McGraw-Hill, New York. 150-163.

Kadowaki M., Yano A., Ishizu F., Tanaka T. and Noda S. (2012), Effects of greenhouse photovoltaic array shading on Welsh onion growth. *Biosystems Engineering.* 111 290-297.

Minuto G., Bruzzone C., Tinivella F., Delfino G. and Minuto A. (2009),. Fotovoltaico sui tetti delle serre per produrre anche energia. *Suppl L'Inform Agrario.* 65(10) 16–9.

Mitalas G.P. and Arseneault J.G. (1972), *FORTRAN IV Program to Calculate z-Transfer Functions for the Calculation of Transient Heat Transfer Through Walls and Roofs*, Division of National Research Council of Canada, Ottawa.

Peng J., Curcija D.C., Lu L., Selkowitz S.E., Yang H. and Mitchell R. (2015), Developing a method and simulation model for evaluating the overall energy performance of a ventilated semi-transparent photovoltaic double-skin façade. *Progress in Photovoltaics: Research and Applications.*

PSE (Projects in Solar Energy) (2009), *Indoor Test Stand for Solar Thermal Collectors – Technical Description.* Freiburg, Germany.

Robinson L. (2009), *Numerical and experimental study of semi-transparent photovoltaics integrated into commercial building façades.* Master's Thesis, Concordia University, Canada.

SketchUp, 2015. http://www.sketchup.com/

Stephenson D.G. and Mitalas G.P. (1971), *Calculation of Heat Conduction Transfer Functions for Multi-Layer Slabs.* ASHRAE Annual Meeting, Washington, D.C., August 22-25.

Skoplaki E. and Palyvos J.A. (2009), On the temperature dependence of photovoltaic module electrical performance. A review of efficiency/power correlations. *Solar Energy.* 83(5) 614–624.

TESS (Thermal Energy System Specialists) (2014), *Library Mathematical Reference.* Component Libraries for the TRNSYS Simulation Environment.

Tritec (2015), http://www.tritec-energy.com/en/reference-cases/1290-greenhouse-cruas/

TRNSYS (2005), *Multizone Building modeling with Type56 and TRNBuild.* Solar Energy Laboratory, University of Wisconsin-Madison, USA.

TRNSYS (2012), *TRNSYS 17 Documentation*, Solar Energy Laboratory, University of Wisconsin-Madison, USA. http://www.trnsys.com/

Ureña-Sánchez R., Callejón-Ferre Á.J., Pérez-Alonso J. and Carreño-Ortega Á. (2012), Greenhouse tomato production with electricity generation by roof-mounted flexible solar panels. *Scientia Agricola.* 69(4) 233–9.